PVT of amorphous and crystalline polymers and their nanocomposites

Utracki, L. A.

Publisher's version / Version de l'éditeur:
https://doi.org/10.1016/j.polymdegradstab.2009.07.020
Polymer Degradation and Stability, 95, March 3, pp. 411-421, 2010

Polymer Degradation and Stability xxx (2009) 1–11

Contents lists available at ScienceDirect

Polymer Degradation and Stability

journal homepage: www.elsevier.com/locate/polydegstab

PVT of amorphous and crystalline polymers and their nanocomposites

L.A. Utracki*

National Research Council Canada, Industrial Materials Institute, 75 de Mortagne, Boucherville, QC J4B 6Y4, Canada

ARTICLE INFO

Article history:
Received 2 March 2009
Received in revised form
10 July 2009
Accepted 15 July 2009
Available online xxx

Keywords:
PVT
Thermal expansion coefficient
Compressibility coefficient
Polyamide-6
Polystyrene
Nanocomposites

ABSTRACT

The Pressure–Volume–Temperature (*PVT*) of polystyrene (PS), polyamide-6 (PA-6) and their clay-containing polymeric nanocomposites (CPNC) were determined at $T = 300$–600 K and $P = 0.1$–190 MPa, thus in the molten, glassy and semicrystalline phase. The melt and glass behavior was interpreted following the Simha–Somcynsky (S–S) cell-hole free volume theory while that of the semicrystalline phase using S–S and the Midha–Nanda–Simha–Jain (MNSJ) cell theory describing crystalline quantum interactions. The theoretical analysis yielded two sets of the interaction parameters, one from the S–S and the other from the MNSJ model. The derivative properties: the compressibility, κ, and thermal expansion coefficient, α, were computed as functions of T, P and clay content, w. These functions, crossing several transition regions, were significantly different for the amorphous PS than for the semicrystalline PA-6. The isobaric PS plots of κ and α *vs.* T detected secondary transitions at $T_\beta/T_g \approx 0.9 \pm 0.1$ and at $T_c/T_g = 1.2 \pm 0.1$. Addition of clay severely affected the vitreous phase (physical aging). In PA-6 systems the behavior was distinctly different than in PS, viz. $\kappa = \kappa(T)$ followed a similar function across the melting zone, while $\alpha = \alpha(T)$ dependencies were dramatically different for the solid and molten phase. The theoretical functions in reduced variables $\tilde{\kappa} = \kappa P^* = \tilde{\kappa}(\tilde{T}, \tilde{P})$; $\tilde{\alpha} = \alpha T^* = \tilde{\alpha}(\tilde{T}, \tilde{P})$ provided good basis for explanation of the observed dependencies.

1. Introduction

Addition of a small quantity of exfoliated and randomly dispersed nano-sized platelets induces large change of material performance, *e.g.*, the Young modulus of a glassy, semicrystalline thermoplastic and elastomeric polymer with 1-wt% clay increases by 3, 20, and 90%, respectively [1,2]. A spectrum of clay-containing polymeric nanocomposites (CPNC) with interesting properties might be prepared using a variety of polymeric matrices, natural and synthetic nanoparticles, intercalants and compatibilizers. Furthermore, the CPNC performance also depends on the method of preparation, thus on morphology, the degree of clay exfoliation, effective aspect ratio, p, the thermodynamic interactions between components and their thermal stability. Because of this great assortment of properties, the theoretical or molecular modeling studies should go parallel with the experimental studies. The Pressure–Volume–Temperature (*PVT*) measurements combined with analysis of data based on sound theoretical principles offers unique insight into the equilibrium and non-equilibrium thermodynamics.

Traditionally, the *PVT* measurements have been carried out for determining the compressibility and the thermal expansion coefficients (κ and α, respectively):

$$\kappa \equiv (\partial \ln V/\partial P)_{T,P^0,q}; \quad \alpha \equiv (\partial \ln V/\partial T)_{T^0,P,q} \tag{1}$$

where P^0 and T^0 are solidification pressure and temperature, respectively, and q is the rate of heating or compressing. Knowledge of these coefficients is essential for the production and engineering application of polymers. As the quantitative theories became available [3–7], *PVT* data also have been used for extracting the thermodynamic information of the system, *e.g.*, the free volume content and/or the binary interaction parameters [8–12].

This article follows the keynote lecture at the MoDeSt 2008 conference where the recent progress in measurements and analyses of the *PVT* behavior for matrix polymers and their CPNC wave been summarized. The customary treatment of the molten phase was extended to the vitreous and crystalline ones, focusing on the significant differences behavior of the amorphous and semicrystalline systems; the derivatives, κ and α, have been computed as well.

2. Fundamentals

The thermodynamic description of the liquid (molten) phase by Simha and Somcynsky (S–S) is based on lattice-hole theory with

* Tel.: +1 450 641 5182; fax: +1 450 641 5105.
E-mail address: TUleszek.utracki@cnrc-nrc.gc.caUT

0141-3910/$ – see front matter Crown Copyright © 2009 Published by Elsevier Ltd. All rights reserved.
doi:10.1016/j.polymdegradstab.2009.07.020

"optimized" h-fraction of empty cells providing a measure of structural disorder. The volume fraction of occupied sites is $y = 1 - h$. The statistical theory is general, derived as Helmholtz free energy, F, for spherical and chain molecule fluids, but mainly know in its derivative version as the equation of state, eos [3,4]:

$$\tilde{P} \equiv -\left(\partial \tilde{F}/\partial \tilde{V}\right)_T \Rightarrow \tilde{P}\tilde{V}/\tilde{T} = (1-U)^{-1} + 2yQ^2\left(AQ^2 - B\right)/\tilde{T} \qquad (2)$$

$$\left(\partial \tilde{F}/\partial y\right)_{\tilde{V},\tilde{T}} = 0 \Rightarrow 3c\left[(U-1/3)/(1-U) - yQ^2\left(3AQ^2 - 2B\right)/6\tilde{T}\right] + (1-s) - (s/y)\ln(1-y) = 0 \qquad (3)$$

where $Q = (y\tilde{V})^{-1}$, $U = 2^{-1/6}yQ^{1/3}$, $A = 1.011$ and $B = 1.2045$ (face-centered cubic lattice).

Eq. (3) was obtained by minimization of $F = F(y)$ and is only valid at the thermodynamic equilibrium. The tilde-marked corresponding states variables in the reduced form are:

$$\tilde{P} = P/P^*; \quad \tilde{T} = T/T^*; \quad \tilde{V} = V/V^*; \quad \text{where}$$

$$P^* = zq\varepsilon^*/sv^*; \quad T^* = zq\varepsilon^*/Rc^*; \quad V^* = v^*/M_s \qquad (4)$$

The Lennard–Jones (L–J) interaction parameters (the maximum attractive energy, ε^*, and the segmental repulsion volume, v^*) are expressed per statistical segment with molar mass $M_s = M_n/s$ (M_n is the number-average molecular weight and s is the number of segments). The parameter $3c$ indicates the external, volume-dependent degrees of freedom; $R = 8.314472$ (J/K mol) is the gas constant; and $zq = s(z-2) + 2$ is the number of interchain contacts in a lattice of the coordination number z, usually taken as 12.

Cooling or compressing polymer melt below the glass transition temperature, T_g, causes its vitrification with different structures and properties, depending on q, P^0 or T^0 [13]. Simha and his collaborators have shown that while Eq. (3) is applicable only to systems under thermodynamic equilibrium, Eq. (2) may be used at the temperature range: $T_\beta \approx 0.75 \times T_g \le T \le T_g$ (T_β is the first sub-T_g transition temperature) assuming that at $T \le T_g$ a part of free volume is "frozen" [12,14–18]. For different polymers the frozen fraction of free volume, FF, decreases with the characteristic reducing temperature, T^*. As the temperature decreases below T_β several secondary transitions make the theoretical description difficult. In consequence, at $0 < T < T_g$ two regions have been theoretically considered: the one near T_g and another neat $T \to 0$ K. The interpretation of material behavior within the first region is based on the assumption of a two-phase system – a liquid-like with compressible free volume fraction, and solid-like where the free volume is "frozen". This image of the glassy region closely resembles the recently proposed by Wool twinkling fractal theory (TFT) [19]. The second region was theoretically described by Simha *et al.* The authors adopted the Lennard–Jones cell theory, postulating that at the very low temperatures the inter-segmental interactions follow the Einstein's quantum equation for the harmonic oscillators [20]. The derived corresponding states (with the Einstein reduced quantum temperature, $\tilde{\Theta}_E = 0.005$) were found valid for several chemically different polymers. Excellent agreement between the theory and experiments was demonstrated for the ambient P data at $T < 80$ K, or $\tilde{T} = 0.004$ ($T \le 80$ K corresponds to the lowest transition temperature in high polymers).

The thermodynamics of the crystalline polymers have been described using either the Grüneisen parameter [21], γ_G, or a statistical thermodynamic theory of solid polymers. Midha and Nanda introduced into the Prigogine's cell model the harmonic and anharmonic interactions for crystalline species [5]. Simha and Jain incorporated into the resulting theory the earlier derived expression for the oscillation frequency near $T \to 0$, ν_0 [6–8]. The final Midha–Nanda–Simha–Jain (MNSJ) model leads to simple expression with five parameters: P^*, T^*, V^*, c/s and ν_0:

$$\begin{aligned}\tilde{P}\tilde{V} &= (2/\tilde{V}^2)\left[(A/\tilde{V}^2) - B\right] + 3\gamma_G F_1(\tilde{\theta},\tilde{T}) \\ &\quad - (9s/4c)ab\tilde{V}^2\tilde{\theta}'^2\left[\frac{1}{2} + \frac{2X}{(X-1)^2}\right] \\ &\quad + (9s/8c)\gamma_G b\tilde{V}^2\tilde{\theta}'^2\left[\frac{1}{2} + \frac{3X+1}{(X-1)^2} - (\tilde{\theta}/\tilde{T})\frac{X(3+X)}{(X-1)^3}\right] \end{aligned} \qquad (5)$$

The secondary functions in Eq. (5) are defined as:

$$\begin{aligned} F_1(\tilde{\theta},\tilde{T}) &= \tilde{\theta}\left[\frac{1}{2} + \frac{1}{X-1}\right]; X(\tilde{\theta},\tilde{T}) = \exp\{\tilde{\theta}/\tilde{T}\} \\ \gamma_G &= \gamma_{G,0}\left\{1 - (s/2c)b\tilde{V}^2\left[F_1(\tilde{\theta}_0,\tilde{T}) - (\tilde{\theta}_0^2/\tilde{T})\frac{X_0}{(X_0-1)^2}\right]\right\} \\ &\quad -(s/c)ab\tilde{V}^2F_1(\tilde{\theta}_0,\tilde{T}) \\ \gamma_{G,0} &= -(\partial \ln v_0/\partial \ln V)_T = 4/3 + A_1/(A_1 - 2B_1V^2) \\ \tilde{\theta}' &= \tilde{\theta}'\left[1 + (3s/8c)b\tilde{V}^2\tilde{\theta}'\right]; \quad \tilde{\theta}' = \tilde{\theta}_0\left[1 + (4/3)(\tilde{T}/\tilde{\theta}_0^2)\right. \\ &\quad \left.\times F_1(\tilde{\theta}_0,\tilde{T})Y\right] + 0(Y) \\ Y &= (3s/8c)\left(\tilde{\theta}_0/\tilde{\theta}'\right)^2\left(\tilde{\theta}_0\tilde{T}\right)^2 b/\tilde{T}; \quad b = \left[(A_2/\tilde{V}^2) - 2B_2\right] \\ &\quad /\left[(A_1/\tilde{V}^2) - 2B_1\right]^2 \\ a &= 1 - \frac{A_2}{(A_2 - 2B_2\tilde{V}^2)} + \frac{2A_1}{(A_1 - 2B_1\tilde{V}^2)}; \\ \tilde{\theta}_0 &= hv_0/kT^* = 4.794 \times 10^{-11}v_0/T^* = 13.189V_0^{-4/3} \\ &\quad \times \frac{\left(A_1/2V_0^2 - B_1\right)^{1/2}}{M_0^{5/6}\sqrt{T^*\sqrt[3]{V^*}}} \\ A_1 &= 22.1060, B_1 = 5.2797, A_2 = 200.653 \text{ and } B_2 = 14.334 \end{aligned} \qquad (6)$$

The relations, Eqs. (2)–(6) have been derived for single-component systems. Since CPNC may be treated as a binary mixture of matrix and solid particles, the Simha-Jain derivation for binary systems needs to be incorporated [22–25]. Accordingly, the scaled Eqs. (2) and (3) retain their validity, but their interaction parameters ε^* and v^* are now compositional averages, $<\varepsilon^*>$ and $<v^*>$, over 11, 22 and 12 binary interactions. The site fractions X_i is defined in terms of the mole fractions x_i:

$$X_i = q_i z x_i / \sum q_i z x_i / \sum q_i x_i; \quad x_i = s_i / \sum s_i \qquad (7)$$

Then the averages $<\varepsilon^*>$ and $<v^*>$ are related to the binary interactions:

$$\left\langle \varepsilon^* \right\rangle \left\langle v^* \right\rangle^p = X_1^2 \varepsilon_{11}^* v_{11}^{*p} + 2X_1X_2\varepsilon_{12}^* v_{12}^{*p} + X_2^2\varepsilon_{22}^{*p}; \quad p \in [2,4] \qquad (8)$$

For molten CPNC the "hairy clay platelet" (HCP) model has been formulated [26]. The model incorporates the reduction of molecular mobility near high-energy crystalline surface. The theory and experiments reveal the presence of solidified organic molecules to a thickness of $z_1 \approx$ 2–9 nm, followed up by a second layer ($z_2 \approx$ 100–120 nm) with progressively increasing mobility [27–30]. As a consequence, one should define the two–component in the binary model of CPNC. The first component with the L–J interaction parameters, ε_{11}^* and v_{11}^*, is the matrix at a distance from the clay surface, $z > z_1$, while the second component with ε_{22}^* and v_{22}^* are the

Please cite this article in press as: Utracki LA, *PVT* of amorphous and crystalline polymers and their nanocomposites, Polym Degrad Stab (2009), doi:10.1016/j.polymdegradstab.2009.07.020

clay platelets with, for PS or PA-6, respectively $z_1 \approx 4$ or 6 nm thick layer of solidified molecules. In other words, the matrix is molten polymer comprising the bulk properties and the layer with reduced mobility at $z_1 \le z < z_2$, whereas the dispersed solids contain inorganic and solidified on it organic parts. An exponential function was adopted for describing the changes of interaction parameters with distance from the clay surface, $\varepsilon_{ii}^*(z)$ or $v_{ii}^*(z)$ [10]:

$$y(z) = \frac{y_1 y_2}{y_1 - (y_1 - y_2)\exp\{n[(z - z_1)/(z - z_2)]\}};\ z_1 \le z < z_2;\quad y \in [\varepsilon^*, v^*] \tag{9}$$

Thus, the interactions of solidified polymer layer at z_1 is expressed as y_1 while at large values of $z \approx z_2$ the exponential term becomes negligible compared to y_1 and y approaches a constant value of y_2, characteristic for the bulk polymer. The amount of molten polymer with bulk properties decreases with the clay content, vanishing at relatively low concentration of $w_1 \approx 0.99$ wt%.

3. Measurements

Details of the experimental procedures and methods of data treatment have been described in the original publications [8–12]. Table 1 lists compositions and selected properties of polystyrene (PS) and poly-ε-caprolactam (PA-6) as well as their CPNC. *PVT* surfaces were measured in a Gnomix pressure dilatometer (Gnomix Inc., Boulder, CO), at $P = 0.1$–190 MPa and $T = 300$–520 or 300–600 K, for PS and PA-6 samples, respectively. The samples were dried for 48 h at 80 °C and their V under ambient condition was determined with accuracy of $\Delta V \le \pm 0.001$ mL/g by the immersion method [31]. Dry pellets were loaded into the dilatometer, pressurized to 10 MPa, pre-molded at $T > T_g$, thus above 400 and 500 K for PS and PA-6, respectively. After 10 min at that T and P the specimen was cooled to ca. 300 K at a rate of 2.5 K/min. For reliability, each sample was measured up to six times. The "standard" test procedure was followed, starting at the ambient T and P, and then measuring $\Delta V = V(P)$ at 30 MPa intervals, next increasing T by 10 K and repeating the process up to the highest set T [31]. The average error in V was less than 0.03%. The run time ranged from 18 to 32 h.

Examples of the *PVT* data for CPNC containing 2-wt% clay in PS and PA-6 are displayed in Figs. 1 and 2, respectively. In these plots the P-dependent transitions (T_g in Fig. 1 and T_m in Fig. 2) are evident, but the secondary transitions are not.

The κ and α coefficients were determined by two methods: (1) direct differentiation of the experimental data ln V (at constant T or P) vs. P or T using the MicroMath Scientist Stineman's cubic spline differentiation [40], and (2) indirect, by fitting the ln$V$ data to a polynomial function of P or T and then differentiating the latter. Since the cubic spline differentiation involves fitting 9 data points and then differentiation the transient curve, the results are "noisy" near the start, finish and transitions. The second method fits the single phase data, smoothing out the experimental noise as well weak secondary transitions. Away from the transitions the κ and α coefficients computed by the two methods were numerically equivalent. As demonstrated in Figs. 3 and 4 the derivative properties of the amorphous and semicrystalline polymers are strikingly different.

Table 1
Polymers and CPNC characteristics.

No.	Code[a]	Clay (wt%)	d_{001} (nm)[b]	m (−)[c]	Exfoliation (%)[d]	References
Polystyrene and its nanocomposites						
1	PS	0	–	–	–	[32]
2	CPNC-1	1.4	4.90	3.3	36	[11,12,33–35]
3	CPNC-2	2.8			27	
4	CPNC-5	5.7	4.02	3.7	14	
5	CPNC-10	10.6	4.18	3.3	12	
6	CPNC-17	17.1			–	
Polyamide-6 and its nanocomposites						
7	PA-6	0	–	–	–	[8,9,26,36,37]
8	PNC-2	2.3	5.88 ± 0.08	<2	93 ± 4	
9	PNC-5	4.9	5.62 ± 0.28	<3	39 ± 16	

[a] CPNC = melt compounded PS + Cloisite 10A (MMT pre-intercalated with dimethyl benzyl hydrogenated tallow ammonium). PNC = polymerization of caprolactam in the presence of MMT pre-intercalated with ω-amino dodecanoic acid [38,39]
[b] Interlayer spacing by XRD.
[c] Number of clay platelets in stack (XRD).
[d] Exfoliation (XRD) – see references.

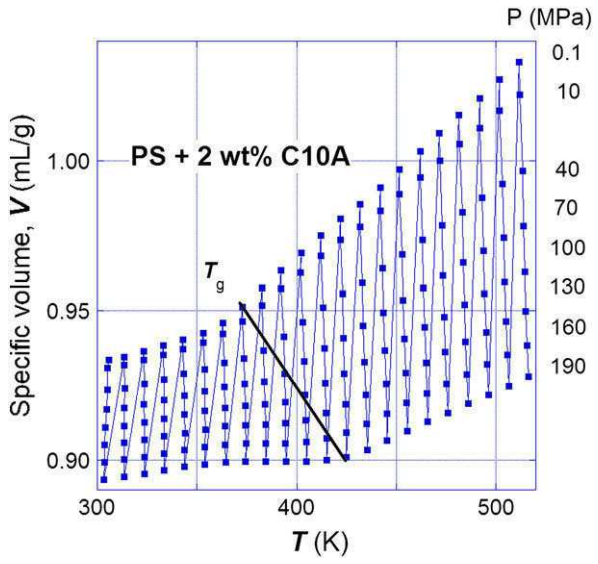

Fig. 1. Specific volume vs. T at $P = 0.1$–190 MPa for CPNC-2. The oblique solid line indicates the glass transition temperature, $T_g = T_g(P)$. The experimental data points are connected by thin dotted line indicating the standard sequence of data acquisition from the lowest to the highest T & P.

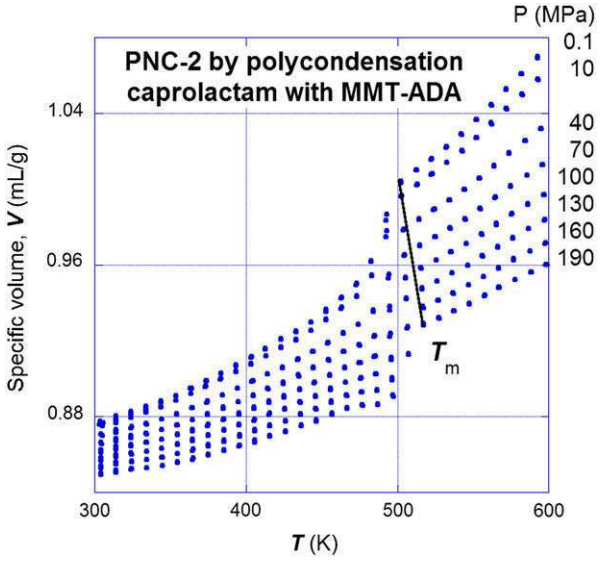

Fig. 2. Specific volume vs. T at $P = 0.1$–190 MPa for PNC-2. Note the excellent superposition of data for the two consecutive runs. The P-dependent melting temperature is indicated.

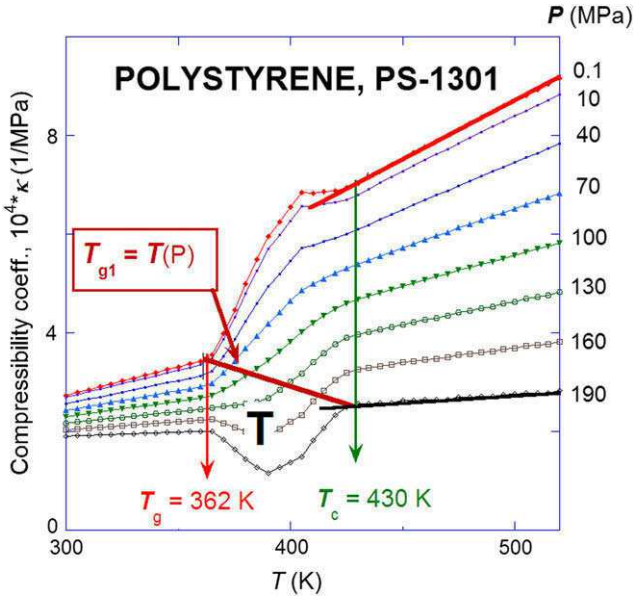

Fig. 3. Isobaric compressibility coefficient of neat PS vs. T at $P = 0.1$–190 MPa. The two arrows show the limit of the glass transition region, whereas the oblique solid line indicates $T_g = T_g(P)$.

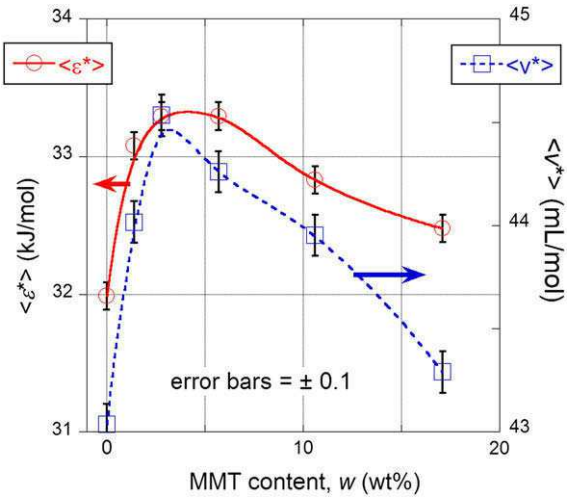

Fig. 5. The bulk-average values of the Lennard–Jones interaction parameters of PS and its CPNC vs. clay content. The local maximum of both functions is at $w_{max} = 3.6$ wt% MMT.

4. Results and discussion

4.1. PS-based CPNC – melt and glass

4.1.1. Melt

The experimental details and discussions may be found in [11,12,14,32–35]. Fitting the *PVT* data Eqs. (2) and (3) provided the volume-average L–J parameters and the free volume function, $h = h(T, P, w)$. Examples of thus extracted functions are displayed in Figs. 5 and 6, respectively. Characteristically, the dependencies pass through a local maximum at $w_{max} = 3.6$-wt% (*viz.* insert in Fig. 6). At this concentration all PS macromolecules are adsorbed by clay stacks into solidified 4 nm thick layer. Further addition of organoclay only dilutes the system with clay and intercalant (25% intercalant excess is in C10A).

The bulk-average L–J parameters in Fig. 5 were converted by means of Eq. (7)–(9) to the binary interaction quantities $\varepsilon^*_{ij}, v^*_{ij}$ (listed in Table 2); the correlation coefficient was: $r^2 = 0.99997$. Owing to the adopted HCP model the matrix is a mixture of molten PS and intercalant, whereas solid particles are composed of clay with bonded to it intercalant and ca. 4 nm thick layer of solidified macromolecules [11,12].

4.1.2. Glass transition; T_g and h_g

As evident from data in Fig. 1, T_g increases with P and decreases with C10A loading (Fig. 7). Another important function of the T_g region is h_g – the free volume quantity at T_g. Its value was calculated

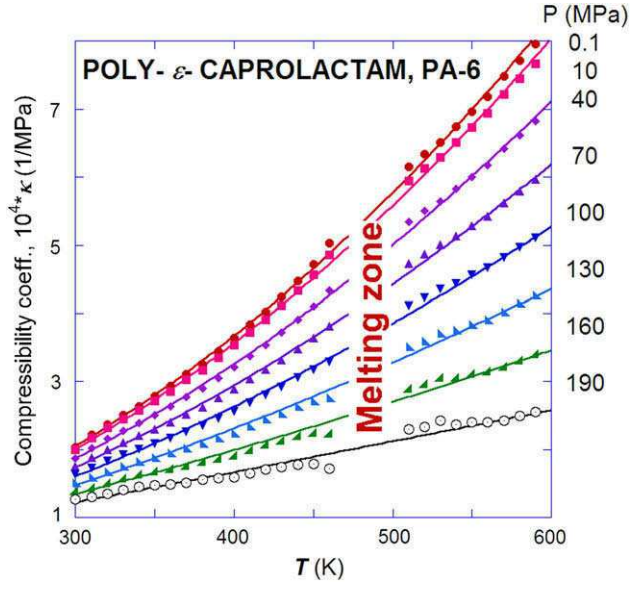

Fig. 4. Isobaric compressibility coefficient of neat PA-6 vs. T at $P = 0.1$–190 MPa. Points were computed by Stineman method, the lines are polynomial, to guide an eye. The melting zone is indicated.

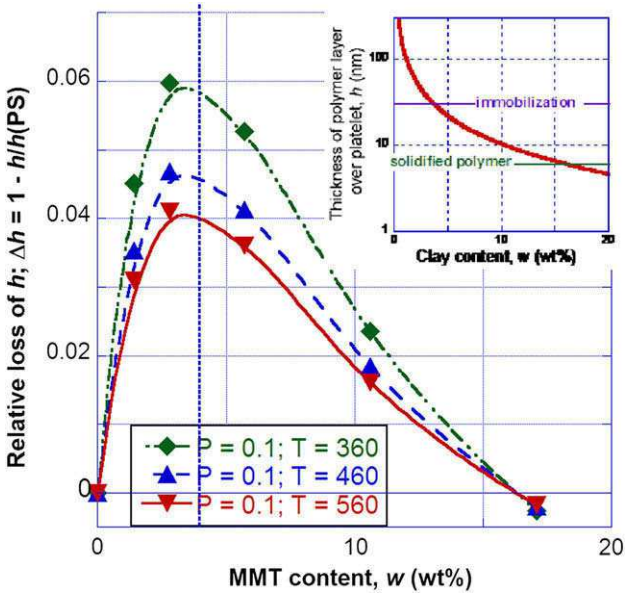

Fig. 6. The relative loss of free volume vs. w at $T = 360$, 460 and 560 K. Points were computed, the lines are to guide an eye. The insert indicates the calculated thickness of adsorbed PS. The local maximum of the functions is at $w_{max} = 3.6$ wt% MMT.

Please cite this article in press as: Utracki LA, *PVT* of amorphous and crystalline polymers and their nanocomposites, Polym Degrad Stab (2009), doi:10.1016/j.polymdegradstab.2009.07.020

Table 2
The L–J binary interaction parameters for PS and PA-6 based CPNC [12,36].

Matrix	Parameters	Binary interactions		
		Matrix/Matrix	Matrix/Solid	Solid/Solid
PS	ε^*	32.0 ± 0.6	32.5 ± 0.4	33.0 ± 0.1
PS	v^*	43.0 ± 1.7	43.6 ± 0.9	44.2 ± 0.1
PA-6	ε^*	34.1 ± 0.3	32.6 ± 0.3	31.2 ± 0.3
PA-6	v^*	32.0 ± 0.1	28.8 ± 0.3	25.9 ± 0.3

from Eqs. (2) and (3) knowing the bulk-average L–J parameters. Plot of h_g vs. P for each CPNC composition is linear – h_g decreases with P:

$$h_g = h_{g,P=0} - b_1 P; \quad w = \text{const.} \tag{10}$$

Fig. 8 presents the computed values of the two parameters of Eq. (10), $h_{g,P=0}$, and $(\partial T_g/\partial P)_w|_{P=0}$, *vs.* clay content, w. Evidently, there is a local minimum of these functions at $w_{max} \approx 3.6$ wt%.

In 1962 Simha and Boyer [41] proposed two relations involving T_g and α's:

$$(\alpha_l - \alpha_g)T_g \cong 0.110 \pm 0.004 \quad \text{and} \quad \alpha^1 \times T_g \cong 0.164 \tag{11}$$

The derivation was based on the erroneous assumption that T_g is an iso-free volume state. Shortly after it was found that the scaled glass transition $\tilde{T}_g \equiv T_g/T^*$ and h_g significantly vary: $1.84 \le 100 \times \tilde{T}_g \le 3.5$ and $0.98 \le 100 \times h_g \le 9.7$ [42]. As shown in Fig. 9, T_g and h_g are interrelated: $T_g = 108 + 45.1\,h_g - 1.38h_g^2$ ($r^2 = 0.88$).; the new data for PS and its CPNC follow that relation. The plot also suggests that there is low limit for $T_g \approx 100$ K at $h_g = 0$, *i.e.*, close to the observed limit of validity of the Simha et al. quantum eos ($T = 80$ K) [20].

4.1.3. *Vitreous state and* FF

The fundamental assumption for the thermodynamic analysis of the glassy state is that glass is a supercooled liquid with the same set of the L–J interactions as in melt and with the behavior controlled by the free volume. However, supercooling kinetically freezes a portion of the free volume, thus the volume change depends only on the accessible free volume portion. This leads to the definition of the isobaric frozen fraction of free volume as [14,15]:

$$FF_T \equiv 1 - (\partial h/\partial T')_{P,glass}/(\partial h/\partial T')_{P,extrapol} \tag{12}$$

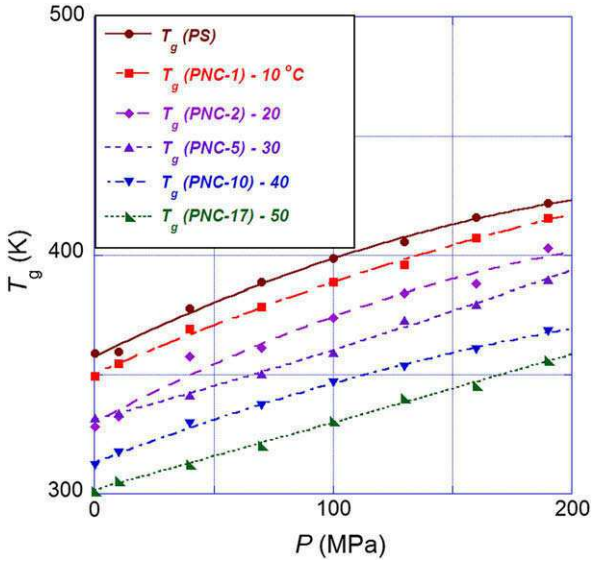

Fig. 7. The glass transition temperature of PS and its CPNC vs. P. For clarity, the data were shifted down by 10 K for the increasing clay content.

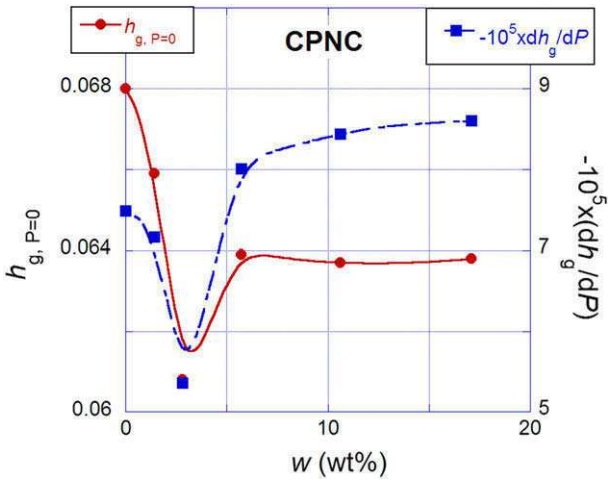

Fig. 8. The free volume at T_g and its pressure gradient vs. w for PS and its CPNC. The local minima of the functions is at $w_{max} = 3.6$ wt% MMT.

where the two partial derivatives represent, respectively, the actual slopes in the vitreous and that extrapolated from the molten region to P and T in the glass; the first one is calculated from the isobaric $V = V(T)$ using Eq. (2), while the second from Eqs. (2) and (3) – in both cases using the characteristic reducing parameters determined from the melt [11,12].

Computed values of $FF = FF(P, w)$ for PS and its CPNC are displayed in Fig. 10. There is a major change of behavior at $w_{max} = 3.6$ wt% – at lower clay content $FF < 1$, whereas at higher $FF > 1$! The magnitude of FF depends on the method of glass preparation (which defines the glass structure) and testing procedure (which determines the way the structure changes) [11]. For neat PS the "standard" *PVT* procedure gave a common dependence: $FF(-) \approx 0.691 + 0.661P$ (P in GPa), shown as a broken line in Fig. 10; the line is close to the FF dependence determined for neat PS. The most intriguing aspect of Fig. 10 is that, for CPNC-5, CPNC-10 and CPNC-17 where $w > w_{max} = 3.6$ wt% clay, $FF > 1$. It is the macromolecular immobilization on clay surface that upon cooling the

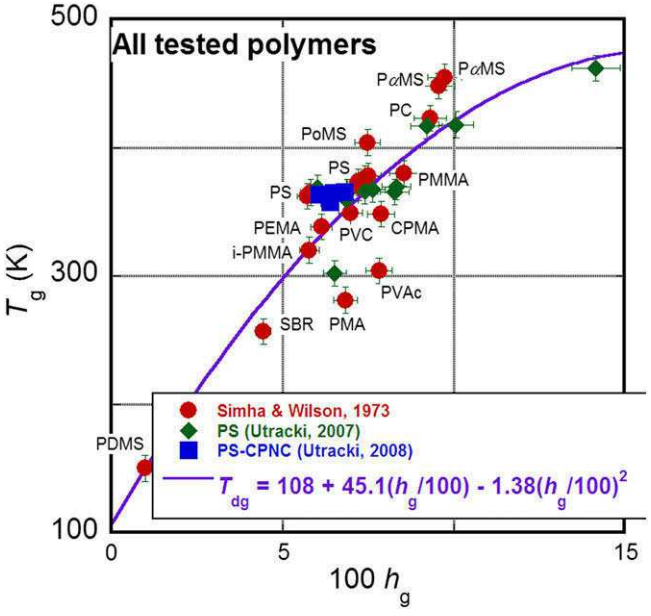

Fig. 9. The glass transition temperature of polymers and nanocomposites vs. the free volume content at T_g. The polynomial fit suggests that the lowest possible value of T_g is about 100 K.

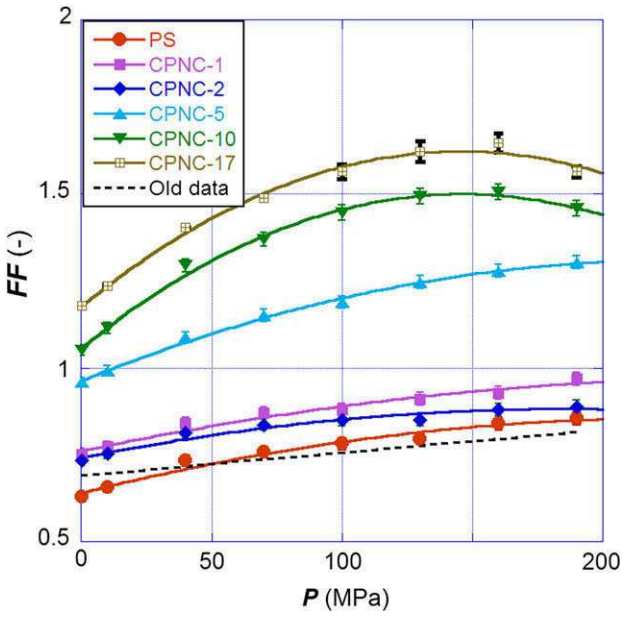

Fig. 10. The frozen fraction of free volume vs. P for the PS-based CPNC. Points were computed, the polynomial lines are to guide an eye. See text.

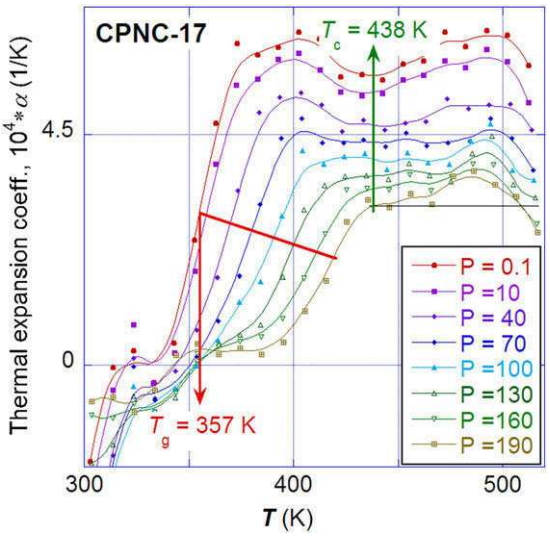

Fig. 12. Isobaric thermal expansion coefficient vs. temperature for PS-based CPNC-17.

melt in the Gnomix pressure dilatometer entraps an excess of free volume, which corresponds to $T \approx T_g + 50$. Upon subsequent re-heating the samples from about 300 K the mobility increases, the free volume decreases and the thermal expansion coefficient becomes negative, $\alpha < 0$ (see Figs. 11and 12 for CPNC-17).

4.1.4. Derivative functions, κ and α

Compressibility and thermal expansion coefficients are complex functions of P, T, and w. Typical plot of $\kappa = \kappa(P, T)$ for PS and its CPNC with 17.1% clay are shown in Figs. 3 and 11, respectively. As T increases the isobaric $\kappa = \kappa(T)$ dependence passes through three regions: I. glassy, II transitory and III molten. Their limits are given by the ambient pressure T_g and crossover temperature, $T_c/T_g \approx 1.25 \pm 0.10$. At low clay concentration κ increases in regions I and III, but it shows a complex behavior in region II.

The glass transition is a cooperative, kinetic process of structural changes [43–45]. The mode-coupling theory (MCT) predicts

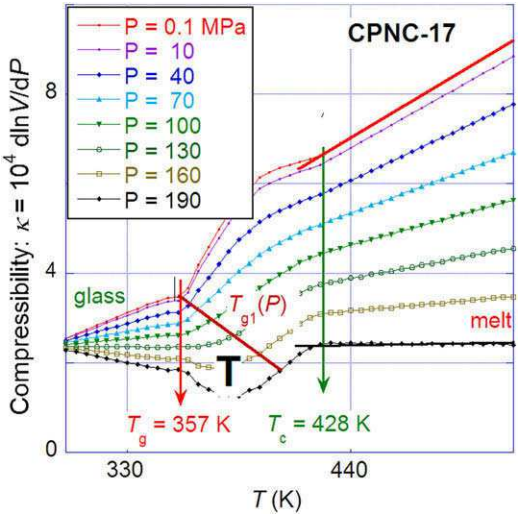

Fig. 11. Isobaric compressibility coefficient as functions of temperature for PS-based CPNC-17.

a change of the relaxation mode at T_c, from the segmental (at $T > T_c$) to structural (at $T < T_c$) [46–49]. The recent twinkling fractal theory, TFT, visualizes cooling molten polymers as a process of dynamic percolation of fractal structures above and below T_g [19]. The solidified polymer fraction is given by:

$$P_s \approx 1 - [(1 - p_c)T/T_g] \tag{13}$$

where p_c is the percolation threshold. Thus, according to TFT there are two temperature limits for the percolating structure to exist: (1) $P_s = 0$ is the initial condition for the solid fractals formation at $T = T_g/(1\text{-}p_c)$ and (2) $P_s = 1$ where the liquid domains disappear at $T \to 0$ K. Eq. (13) also predicts that at T_g the solid fraction attains the percolation level: $P_s \approx p_c$. Thus, according to TFT T_g through p_c, is controlled by dimensionality, packing arrangement and aspect ratio of the segmental aggregates. In other words, T_g depends on other factors than equilibrium thermodynamics and as such it cannot possibly be an iso-free volume state. Accepting the TFT model one may identify *FF* as the fraction of free volume entrapped within the solid "twinkling" fractals with the rest remaining within the molten domains and as such available for expansion and compression.

If the initial cluster formation occurs at T_c, than according to Eq. (13), $p_c \approx 0.20 \pm 0.10$. In 3D structures the regular face-centered cubic (fcc) has the coordination number $z = 12$ and $p_c^{fcc} = 0.1201635 \pm 0.000001$, while the body centered cubic packing (bcc) has $z = 8$ and $p_c^{bcc} = 0.2459615 \pm 0.000001$ [50–53]. Considering that in polymers the most frequently reported value is $p_c \approx 0.16$–0.19 [54,55], the fractal packing may be that of fcc with non-spherical elements.

The direct differentiation of isobaric ln$V$ *vs.* T dependencies was used to calculate α. An example of the plot is displayed in Fig. 12. The $\alpha = \alpha(T,P = \text{const.})$ dependencies also have the same three regions as κ, characterized by nearly constant α_g and α_l separated by region of variable α. At low T the temperature gradient of α_g depends on clay content, at low, $w < w_{max}$, it vary little:$a_g \approx 2.91 \times 10^{-4}$ (1/K), at higher concentrations it decreases with w and for $w > w_{max}$ the expansion coefficient becomes negative. In region III, considering the experimental and computational uncertainties, α_l is independent of T and w, decreasing with P (see Fig. 14). Evidently at $T > T_c$ the effect of polymer adsorption on clay surface is small and the thermal expansion of CPNC depends on the matrix. As it will be shown later this observation is not valid for nanocomposites with semicrystalline PA-6 matrix.

Please cite this article in press as: Utracki LA, *PVT* of amorphous and crystalline polymers and their nanocomposites, Polym Degrad Stab (2009), doi:10.1016/j.polymdegradstab.2009.07.020

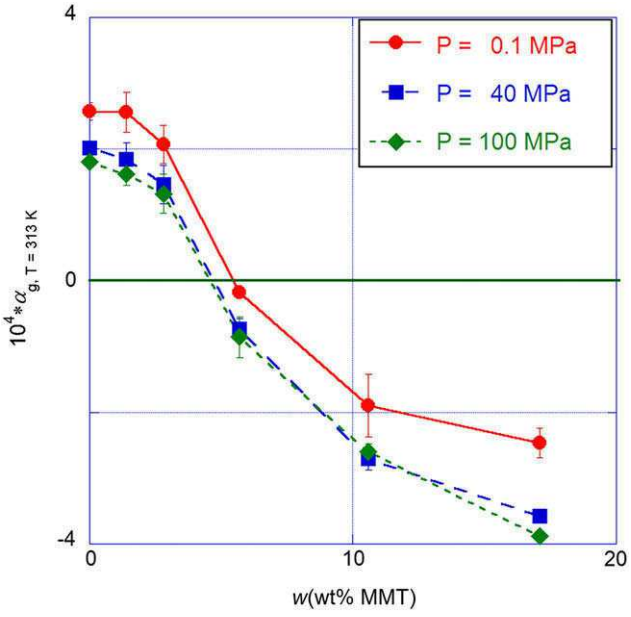

Fig. 13. The thermal expansion coefficient of vitreous PS and its CPNC vs. clay content at three levels of *P*.

4.2. PA-6 based CPNC – molten and solid phase

4.2.1. Melt behavior

The experimental details and discussions may be found in [8,9,26,36,37]. The *PVT* data of the melts was fitted to Eqs. (2) and (3), the bulk L–J parameters were calculated, from which the binary values of ε^*_{ij} and v^*_{ij} were extracted. Their numerical values are listed in Table 2. By contrast with the previous results for commercial PA-6 based PNC [8,9], where addition of clay reduced the free volume content, this time (Fig. 15) an opposite effect was observed. The excess of clay intercalant (ω-amino dodecyl acid, ADA) is responsible for this behavior. ADA simultaneously melts and decomposes at 458–460 K generating large quantity of free volume.

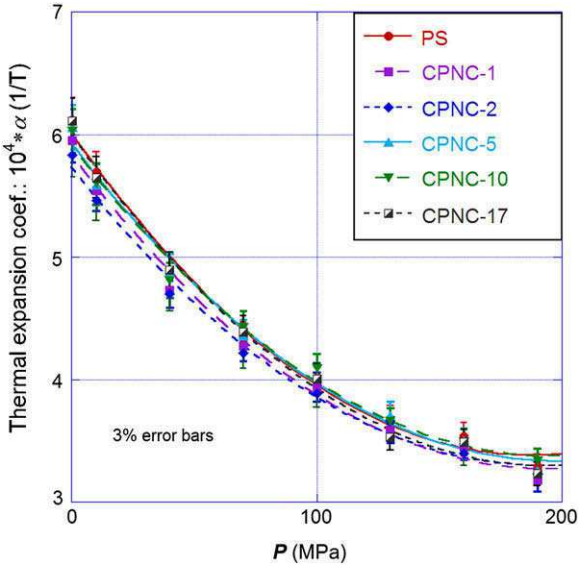

Fig. 14. The thermal expansion coefficient of molten CPNC vs. pressure for PS and its CPNC.

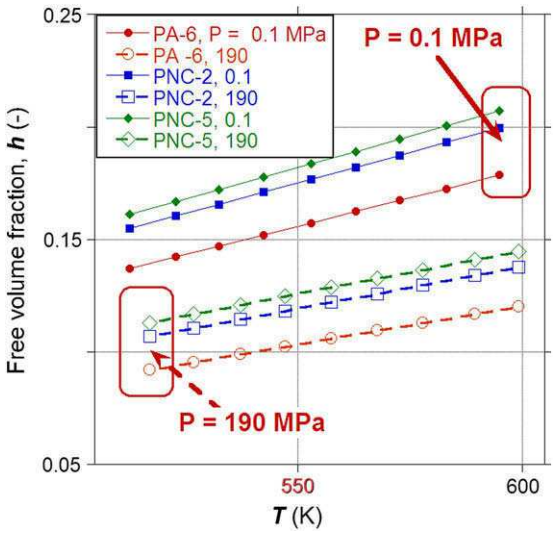

Fig. 15. Free volume quantity, *h*, vs. *T* for PA-6, PNC-2 and PNC-5 at two pressures: $P = 0.1$ and 190 MPa [36,37].

4.2.2. The melting region

The melting region is characterized by three measures: the melting temperature, T_m, the width of the transition zone, ΔT_m and its height ΔV_m [36]. While T_m is the characteristic thermodynamic property of the polymer, ΔT_m and ΔV_m depend on the initial crystallinity and the kinetics of melting and recrystallization during the test. As shown in Fig. 1, in the standard *PVT* test procedure the sample is pressurized isothermally, then the temperature is increased by 10 K and process repeated. Thus, near T_m the sample may be melting at lower *P*, then crystallizing at higher, etc. This usually leads to a wider melting zone than observed during calorimetric scans in, *e.g.*, a differential scanning calorimeter, DSC. The knowledge of ΔV_m is essential for the thermodynamic analysis of the "solid" part in the semicrystalline polymers.

4.2.3. The semicrystalline region

At constant pressure, within the range $T_g \leq T \leq T_m$, PA-6 is a mixture of crystals and liquid polymer; only below T_g the melt vitrifies and one may treat the system as a "solid". Since in the studied PA-6 based systems $T_g \approx 316 \pm 1$ K and the dilatometric measurements start at ca. 300 K, the semicrystalline region was

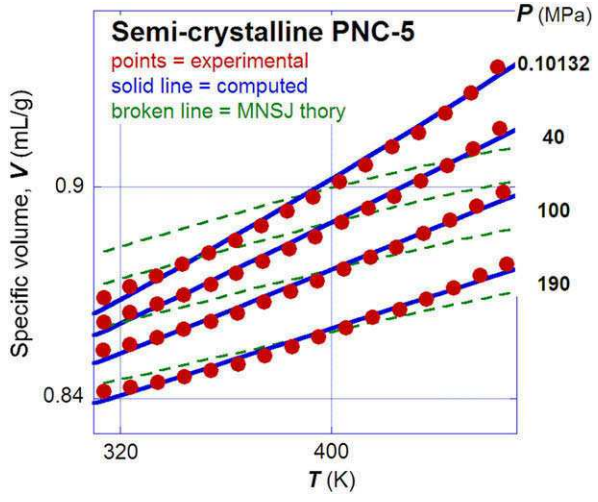

Fig. 16. Specific volume vs. *T* within the semicrystalline region at $T_g \leq T \leq T_m$, for PNC-5 at four indicated pressures.

Please cite this article in press as: Utracki LA, *PVT* of amorphous and crystalline polymers and their nanocomposites, Polym Degrad Stab (2009), doi:10.1016/j.polymdegradstab.2009.07.020

Table 3
Characteristic parameters of PA-6 computed from the MNSJ theory fitted to the crystalline region I and from the S–S eos fitted to the molten region III [37].

Parameter	Region I; MNSJ	Region III; S–S
P^* (MPa)	5531 ± 82	1067 ± 12
T^* (K)	10,349 ± 68	12,282 ± 66
V^*x10^4 (mL/g)	8804 ± 10	9198 ± 16
M_s (g/mol)	17.7 ± 0.7	34.7 ± 0.6
#cells/mer	6.4	3.3
ε^* (kJ/mol)	**28.7 ± 0.3**	**34.1 ± 0.3**
v^* (mL/mol)	**15.6 ± 0.2**	**32.0 ± 0.1**

treated as a mixture of molten organic phase and dispersed in it PA-6 crystals (increasing with P from $X_{cryst} = 15$–40 wt%) and 0, 2.3 or 4.9 wt% clay [36,37]. The equilibrium crystallinity of PA-6 is $X_{eq.cryst} \cong 29 - 31\%$ [56–58].

Consequently, the *PVT* behavior of the semicrystalline region must be interpreted as a combination of melt (Eqs. (2) and (3)) with crystals (Eqs. (5) and (6)). An example of the computations is presented in Fig. 16 where the solid points are experimental and thin broken lines show their fit to the MNSJ theory – the volume of the crystalline phase changes less with T than that of melt (this is reflected in the two sets of the characteristic parameters listed in Table 3). The solid lines in the Figure represent the final results where the experimental behavior is assumed to be an additive combination of melt and dispersed in it PA-6 crystals:

$$V = \Delta V_{m,c} + X_{cryst} V_{solid} + (1 - X_{cryst}) V_{melt} \quad (14)$$

were $\Delta V_{m,c}$ and X_{cryst} are obtained by iteration. The main contribution to the former is ΔV_m, *i.e.*, the volume reduction upon crystallization, other one originates from P-dependent pre-melting, crystallization and annealing, while the final one corrects the error introduced from fitting the crystalline phase behavior to the experimental data of semicrystalline polymer. It is noteworthy that the maximum crystallization rate is expected at: $T_{max} = (T_g + T_m)/2 \approx 405$ K, thus about mid-point of the T-range in Fig. 16 [59].

4.2.4. Derivative functions, κ and α

Fig. 4 displays the compressibility coefficient of PA-6, computed using the Stineman cubic spline differentiation protocol. The coefficients of the other two compositions follow a similar pattern. Omitting the melting zone at $T \approx 470$–500 K, the derivatives below and above it might be represented by the 2nd order polynomial. Thus, the compressibility of PA-6 and its PNC, $\kappa = \kappa(T)$, seemingly is a smooth function across the T_m region. The compressibility coefficient decreases with increasing P – more so for the molten than the solid phase.

The effect of clay addition is small, better seen in the relative compressibility $\kappa_R \equiv k(PNC)/\kappa(PA-6)$. In the molten phase the presence of clay with excess of intercalant increased compressibility of PNC-2 and -5 by about 5%. However, in the semicrystalline phase at low P κ_R decreased by ca. −5 and −10% for PNC-2 and -5, respectively. At high P the $\kappa_R \to 1$, *i.e.*, $\kappa(PNC) \simeq \kappa(PA-6)$[37]. Thus, it is evident that $\kappa \equiv (\partial \ln V/\partial P)_T$ depends mainly of the molten polymer content. This contrasts the κ-behavior in PS systems near T_g – compare Figs. 3 and 4.

Another sharp difference in behavior on two sides of the transition temperature is seen in the isobaric thermal expansion coefficients, $\alpha \equiv (\partial \ln V/\partial T)_P$, of the amorphous and semicrystalline systems. For PS and its CPNC the effects of T, w and P on α is shown in

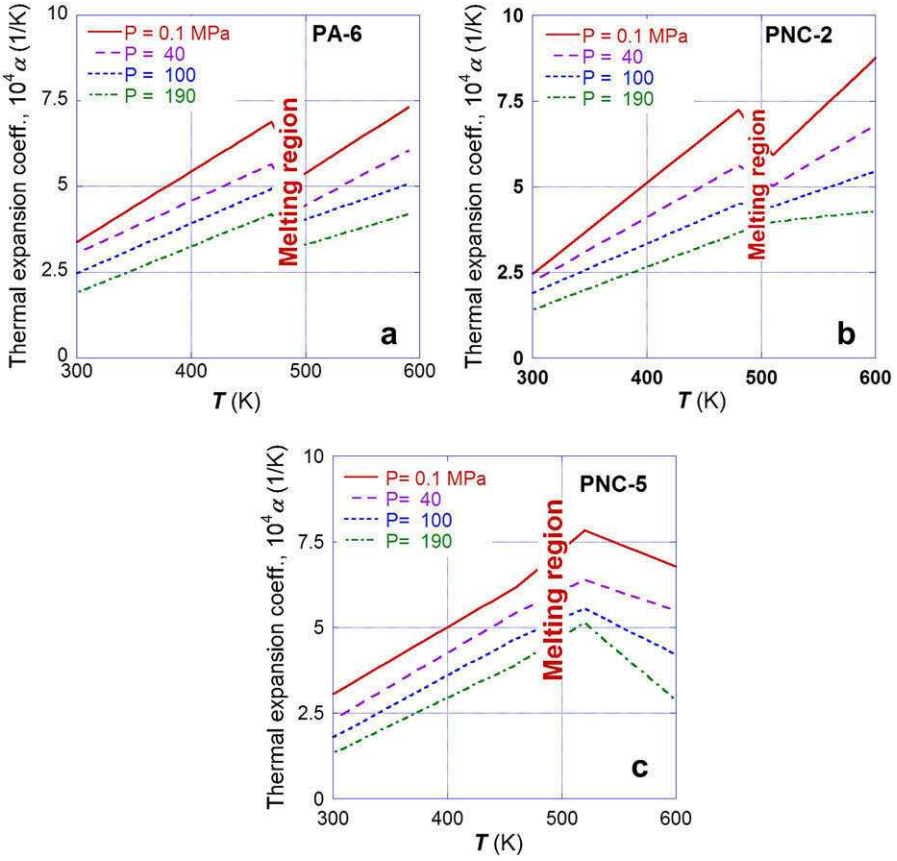

Fig. 17. Schematic dependencies of the isobaric thermal expansion coefficients vs. T for PA-6 and its CPNC at four indicated P. There is remarkable difference of behavior on the two sides of the melting region.

Figs. 12–14, respectively; clay strongly affected α in the glassy region, but not in the molten phase where the coefficient was virtually T-independent. Its T-dependence in PA-6 and its PNC is schematically shown in Fig. 17 [37]. Within the semicrystalline region the $\alpha = \alpha(T)$ of the three compositions are similar, linearly increasing with T for PA-6 and its PNC. The melting zone for the samples occurs at about the same T_m, but its width increases with the clay content. Unexpectedly, increasing T across the molten region reduces α of PA-6 and PNC-2 by *ca.* 40%. Furthermore, clay strongly effects α in the molten region III – the slope $d\alpha/dT$ decreases with increasing w and P. The reduction of the thermal expansion coefficient with increasing T is unexpected as it suggests higher free volume content in the vitreous than in the molten phase.

4.3. Theoretical predictions

The P and T dependencies of V, κ and α indicate significant difference in behavior between the amorphous and semicrystalline polymers and their nanocomposites. The *PVT* behavior of PS follows the S–S cell-hole model for liquids – directly at $T > T_g$ and with the assumption of the frozen free volume at $T < T_g$. In spite of excellent fit of the theoretical equations to $V = V(P, T)$ on both sides of T_g the derivatives, κ and α, indicate the presence of changeable structures within a wide range of T and P.

The behavior of semicrystalline PA-6 and its PNC is more difficult to analyze and interpret. The molten region follows the S–S eos, whereas the semicrystalline one at $T < T_m$ must be treated as a mixture of molten organic phase with dispersed in it PA-6 crystals. Thus, at $T_g < T < T_m$ one needs to use two theoretical models, one based on the free volume the other on the quantum interactions in crystals. Furthermore, the composition of this phase varies with P and T. In PA-6 at $T > T_g$ one should not expect to see transition region similar to that in PS, but intuitively the behavior of κ and α should at least resemble each other. Furthermore, the effect of clay being small in PS-based CPNC was expected to be similarly of low significance on the *PVT* behavior on both sides of T_m – the data disagree with these expectations. Thus, it is important to establish how much of these "disagreements" follows from the theories.

Both S–S and MNSJ theories were numerically differentiated to yield κ and α [37, 60]. The ranges of scaled variables in *PVT* tests are: $\tilde{T}(PS) = 0.026–0.046$; $\tilde{T}^g(PA-6) = 0.024–0.054$, the transition temperatures are: $\tilde{T}(PS)^g = 0.031$; $\tilde{T}_c(PA-6) = 0.037$; and the reduced pressures ranges: $\tilde{P}(PS) = 1.34 \times 10^{-4}–0.256$; $\tilde{T}(PA-6) = 0.822 \times 10^{-4}–0.179$. Evidently, in PS systems the transition region II with changing fractal structure on both sides of T_g cannot be described by the S–S eos, but one should compute the derivatives in the regions I (glass) and III (melt), and then compare the predictions with the experimental dependencies. The computed from Eqs. (2) and (3) derivatives in the scaled form, $\tilde{\kappa} = \kappa P^*$ and $\tilde{\alpha} = \alpha T^*$, are displayed in Figs. 18 and 19, respectively. For the molten region III they were computed directly, whereas those for the vitreous region I assuming that here the fractal structure is reflected in the amount of the frozen and non-frozen free volume, $FF = FF(\tilde{P})$ and $(1 - FF)$, respectively.

Similar analysis of the PA-6 with the first order transition at $\tilde{T}_m(PA-6) = 0.041$ leads to dependencies shown in Figs. 20 and 21. Here again the derivatives in region III were computed directly from Eqs. (2) and (3), while those for the semicrystalline region I considering that contributions from the liquid (from S–S eos) and crystalline phase (from MNSJ eos) are additive:

$$\tilde{\kappa}(\tilde{P},\tilde{T}) = \tilde{\kappa}_{s-s}(\tilde{P},\tilde{T}) + \phi_x(\tilde{P})\left[\tilde{\kappa}_{MNSJ}(\tilde{P},\tilde{T}) - \tilde{\kappa}_{s-s}(\tilde{P},\tilde{T})\right] \quad (15)$$

where $\phi_x(\tilde{P})$ is the volume fraction of the crystalline phase calculated from X_{cryst} in Eq. (14), thus obtained by fitting the dependence

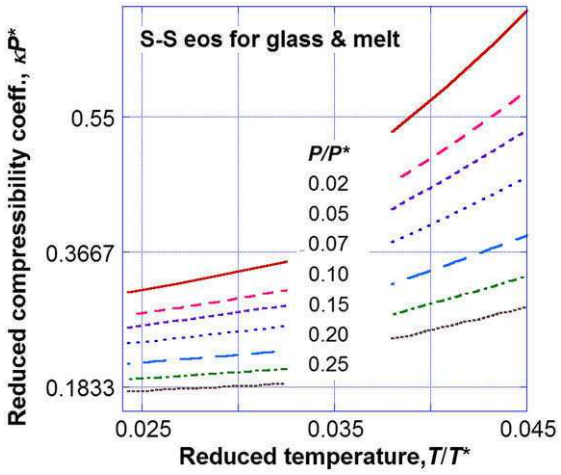

Fig. 18. Isobaric reduced compressibility vs. reduced temperature computed from the S–S eos for PS. The glass transition region II is omitted.

to experimental data for the semicrystalline phase. Similar procedure was used for calculating $\tilde{\alpha}(\tilde{P},\tilde{T})$.

The experimental and theoretical dependencies for PS in Figs. 3 and 18 are in good agreement for κ-dependencies outside the transitional T_g region II. Thus, within the corresponding ranges of independent variables the magnitude of the compressibility coefficient in region I and III is correctly predicted. The experimental data of $\alpha = \alpha(P, T, w)$ are displayed in Figs. 13 and 14. The ambient pressure $\alpha_g \approx 2.6 \times 10^{-4}$ is within the range of values reported for linear polymers $10^4\alpha_g \approx 1.9 \pm 0.9$ [61]. The theoretical dependencies in Fig. 19 show that α is a weakly increasing function of T, making the experimental T-independent values of α in regions I and III acceptable. Comparing the effect of P on α leads to similar conclusions as those made for κ: the effect of P in regions I and III is correctly predicted. For example, in Fig. 13 at $T = 313$ K the value of $\alpha x10^4$ at three pressures changes by a factor of 1.4 (from 2.6 to 1.8), whereas in Fig. 19 the αT^* changes from 4.6 to 3.2, *i.e.*, by the same factor of 1.4. Similarly for the melt, in Fig. 14 $\alpha x10^4$ ranges from about 6.0–3.3, whereas in Fig. 19 αT^* from 7 to 4. In conclusion, S–S eos not only well describes the *PVT* dependence in the molten and vitreous region, but also offers correct predictions of the derivative properties in the full range of the independent variables.

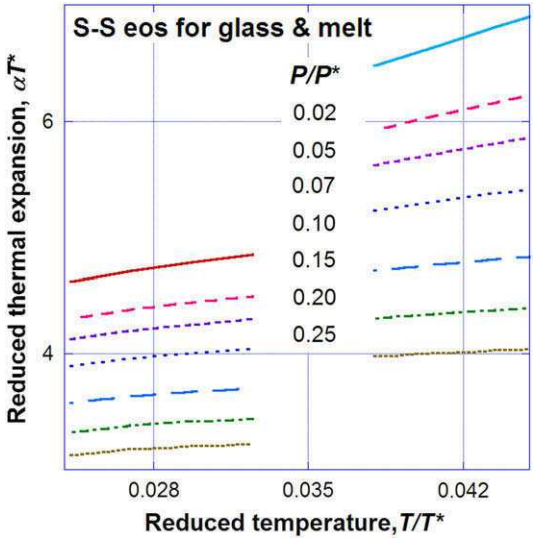

Fig. 19. Isobaric reduced thermal expansion coefficients vs. reduced temperature computed from the S–S eos for regions I and III.

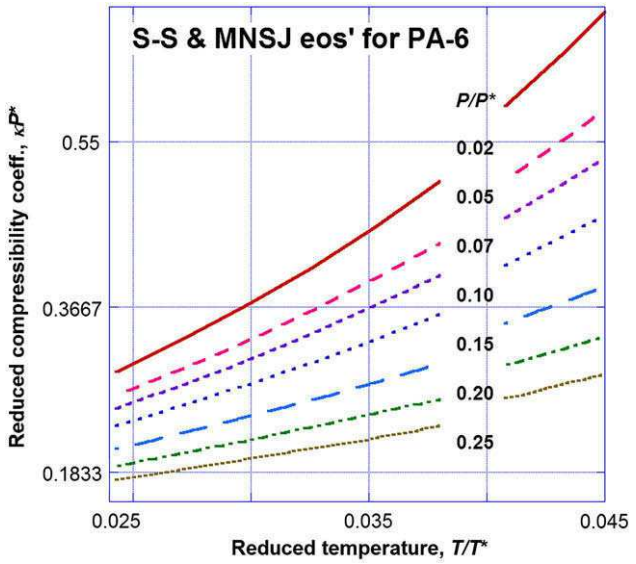

Fig. 20. Pressure dependent reduced compressibility vs. reduced temperature computed from the S–S and MNSJ theories. The melting region II is omitted.

Turning now to PA-6 one notice that the "puzzling" near-continuity of $\kappa = \kappa(T)$ dependence is predicted by the theories. Close comparison of Figs. 4 and 20 shows that in both plots the "continuity" is only approximate; it is better at low P than at high, where in both Figures there is a small step up across the T_m region. Thus, again the S–S eos for the molten region and the combination of S–S with MNSJ eos for the semicrystalline region well predicts the compressibility coefficient. However, this is not so for the thermal expansion where the theory predicts that $\alpha_{melt}T^* > \alpha_{cryst}T^*$ while the experiment shows the opposite $\alpha_{melt} < \alpha_{cryst}$ (see Figs. 17a and 21). There is no doubt that the theoretical prediction better agrees with the common sense – semi-solid body should expand less than liquid. The observed higher $\alpha-$ value in region I indicates a higher free volume content at $T < T_m$ than at $T > T_m$. This could be possible if during crystallization there is significant rarefaction of the amorphous domains adjacent to crystals. Since κ does not show similar changes on melting it means that the rigid crystals (crystallinity increases with P!) are capable to support the pressure. In other word, the presence of structure in semicrystalline phase and its absence in the melt make the direct comparison of the theoretical and experimental magnitudes of α difficult. Addition of clay to PA-6 is responsible for the formation of other structures, evidenced in the volume changes upon crystallization [37].

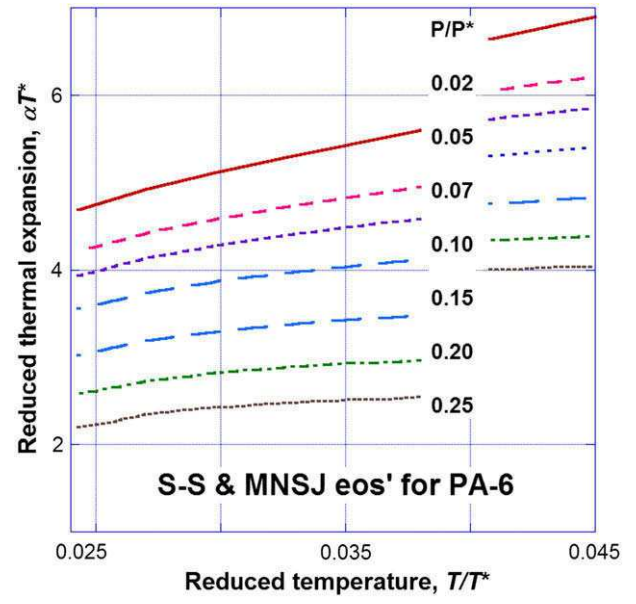

Fig. 21. Pressure dependence of the reduced thermal expansion coefficients vs. reduced temperature computed from the S–S and MNSJ theories. The melting region II is omitted.

5. Summary

This article summarized the recent findings based on the theoretical analyses of the *PVT* polymer behavior by Robert Simha and his colleagues. It examined the variability of *PVT* and its derivatives for amorphous and semicrystalline polymer as well as for their nanocomposites. The experimental derivatives were also compared with theoretical prediction. The findings may be condensed as:

1. Both studied systems, one based on PS and the other on PA-6, have a transition region in the middle of the scanned temperature range; T_g for PS and T_m for PA-6 systems. As a result, there are three regions of behavior: I. Vitreous or semicrystalline; II. Transitory; and III. Molten.
2. The *PVT* data show relatively narrow region II, whereas in the derivative properties its size is significantly wider, *e.g.* for PS systems the region II is defined by the temperature limits given by the glass transition and the crossover point, both at the ambient P, *i.e.*, its width is $T/T_g \approx 1.25$. The recent twinkling fractal theory, TFT, offers good interpretation of the structure and its variability within this region. In the PA-6 systems the size of the transition region II increases with clay content and decreases with P.
3. The *PVT* behavior of PS-based systems is well described by the Simha-Somcynsky cell-hole theory – directly in region III, and with assumption of the partially "frozen" free volume in region I. The postulated by TFT fractal structure offers good explanation for the presence of "free" and "frozen" free volume in the liquid-like and solid-like fractal domains.
4. Similarly, the *PVT* behavior of PA-6-based systems is well described by S–S eos in region III and by combination of S–S and MNSJ eos in region I, where the cell-based MNSJ theory with quantum interactions well describes the thermodynamic behavior of PA-6 crystals.
5. The derivative isobaric functions, $\kappa = \kappa(T)$ and $\alpha = \alpha(T)$, behave differently in PS than in PA-6. In PS both coefficients showed similar tendencies in the three regions, while in PA-6 the compressibility $\kappa = \kappa(T)$ seems to follow the same function across the T_m region, whereas $\alpha = \alpha(T)$ passing from region I to region III is step-wise reduced by $\geq 25\%$.
6. Theoretical values of $\kappa = \kappa(P, T)$ and $\alpha = \alpha(P, T)$ for PS showed good agreement with experimental. Similarly, good agreement was obtained for $\kappa = \kappa(P, T)$ of PA-6, but not for α. It was postulated that this difference originates in rarefaction during crystallization, which induces extra free volume, and the presence of increasing with P crystallinity enable to support the compressive pressure, increasing κ within the semicrystalline region I.
7. Incorporation of clay into PS and PA-6 resulted in different effects. In region III addition of clay to PS had little effect, but severe in PA-6. By contrast, in region I of PS nanocomposites the clay presence severely affected $\kappa = \kappa(T)$ and $\alpha = \alpha(T)$, to the extent of changing the sign of their T-derivatives, while its effect in the semicrystalline PA-6 was negligible.

Please cite this article in press as: Utracki LA, *PVT* of amorphous and crystalline polymers and their nanocomposites, Polym Degrad Stab (2009), doi:10.1016/j.polymdegradstab.2009.07.020

8. Prediction/interpretation of clay effect on matrix behavior needs to consider the presence and content of ALL components of the system, *viz.* matrix, clay, intercalant and the often used compatibilizer. Solidification of organic compounds on clay surface is a rule, but depending on the thermodynamic interactions the matrix polymer may not be the one to be so affected.

Acknowledgment

The author expresses his gratitude for the decades-long collaboration with Robert Simha (1912–2008) and his profound insight into the fundamentals of the thermodynamics of polymeric multiphase systems in the molten, vitreous and solid state.

References

[1] Utracki LA. Clay-containing polymeric nanocomposites. Shawbury, Shropshire: RAPRA; 2004.
[2] Utracki LA. Mechanical properties of clay-containing polymeric nanocomposites. In: Gupta R, Kennel E, Kim KJ, editors. Handbook of polymer nanocomposites. Boca Raton, FL: CRC Press; 2009.
[3] Simha R, Somcynsky T. On the statistical thermodynamics of spherical and chain molecule fluids. Macromolecules 1969;2:342–50.
[4] Somcynsky T, Simha R. Hole theory of liquids and glass transition. J Appl Phys 1971;42:4545–8.
[5] Midha YR, Nanda VS. Equation of state for a polymer crystal. Macromolecules 1977;10:1031–5.
[6] Simha R, Jain RK. Statistical thermodynamics of polymer crystal and melt. J Polym Sci Polym Phys Ed 1978;16:1471–89.
[7] Jain RK, Simha R. High pressure isotherms of polyethylene crystals. J Polym Sci Polym Lett Ed 1979;17:33–7.
[8] Simha R, Utracki LA, Garcia-Rejon A. Pressure–volume–temperature relations of a poly-ε-caprolactam and its nanocomposite. Composite Interfaces 2001;8:345–53.
[9] Utracki LA, Simha R, Garcia-Rejon A. Pressure–volume–temperature relations in nanocomposites. Macromolecules 2003;36:2114–21.
[10] Utracki LA, Simha R. Pressure–volume–temperature dependence of polypropylene/ organoclay nanocomposites. Macromolecules 2004;37:10123–33.
[11] Utracki LA. Pressure–volume–temperature of molten and glassy polystyrene. J Polym Sci Part B Polym Phys 2007;45:270–85.
[12] Utracki LA. Free volume of molten and glassy polystyrene and its nanocomposites. J Polym Sci Part B Polym Phys 2008;46(23):2504–18.
[13] Cowie JMG, McEwen IJ, McIntyre R. In: Utracki LA, editor. Polymer blends handbook. Dordrecht: Kluwer Academic Press; 2002.
[14] Quach A, Simha R. Pressure–volume–temperature properties and transitions of amorphous polymers; polystyrene and poly-o-methyl-styrene. J Appl Phys 1971;42:4592–606.
[15] Quach A, Simha R. Statistical thermodynamics of the glass transition and the glassy state of polymers. J Phys Chem 1972;76:416–21.
[16] McKinney JE, Simha R. Configurational thermodynamic properties of polymer liquids and glasses. I Polyvinyl acetate. Macromolecules 1974;7:894–901.
[17] McKinney JE, Simha R. Configurational thermodynamic properties of polymer liquids and glasses polyvinyl acetate II. Macromolecules 1976;9:430–41.
[18] McKinney JE, Simha R. Configurational thermodynamic properties of polymer liquids and glasses. Polyvinyl acetate. J Res NBS – Phys Chem 1977;81A:283–97.
[19] Wool PP. Twinkling fractal theory of the glass transition. J Polym Sci Part B Polym Phys 2008;46:2765–78.
[20] Simha R, Roe JM, Nanda VS. Low-temperature equation of state for amorphous polymer glasses. J Appl Phys 1972;43:4312–7.
[21] Warfield RW, Kayser EG, Hartmann B. Grüneisen parameter for polyamides. Macromol Chem 1983;184:1927–35.
[22] Simha R, Jain RK, Jain SC, Simha R. Bulk modulus and thermal expansivity of melt polymer composites: statistical versus macro-mechanics. Polym Composites 1984;5:3–10.
[23] Papazoglou E, Simha R, Maurer FHJ. Thermal expansivity of particulate composites: interlayer versus molecular model. Rheol Acta 1989;28:302–10.
[24] Jain RK, Simha R. On the statistical thermodynamics of multicomponent fluids: equation of state. Macromolecules 1980;13:1501–8.
[25] Jain RK, Simha R. Statistical thermodynamics of multicomponent fluids. Macromolecules 1984;17:2663–8.
[26] Utracki LA, Lyngaae-Jørgensen J. Dynamic melt flow of nanocomposites based on poly-ε-caprolactam. Rheol Acta 2002;41:394–407.
[27] Israelachvili JN, Tirrell M, Klein J, Almog Y. Forces between two layers of adsorbed polystyrene immersed in cyclohexane below and above the Θ temperature. Macromolecules 1984;17:204–9.
[28] Horn RG, Israelachvili JN. Molecular organization and viscosity of a thin film of molten polymer between two surfaces as probed by force measurements. Macromolecules 1988;21:2836–41.
[29] Hentschke R. Molecular modeling of adsorption and ordering at solid interfaces. Macromol Theory Simul 1997;6:287–316.
[30] Luengo G, Schmitt F-J, Hill R, Israelachvili JN. Thin film rheology and tribology of confined polymer melts: contrasts with bulk properties. Macromolecules 1997;30:2482–94.
[31] Zoller P, Walsh D. Standard pressure–volume–temperature data for polymers. Lancaster-Basel: Technomic Pub Co; 1995.
[32] Utracki LA. Pressure–volume–temperature dependencies of polystyrenes. Polymer 2005;46:11548–56.
[33] Tanoue S, Utracki LA, Garcia-Rejon A, Tatibouët J, Cole KC, Kamal MR. Melt compounding of different grades of polystyrene with organoclay: part 1 compounding and characterization. Polym Eng Sci 2004;44:1046–60.
[34] Tanoue S, Utracki LA, Garcia-Rejon A, Sammut P, Ton-That M-T, Pesneau I, Kamal MR, Lyngaae-Jorgensen J. Melt compounding of different grades polystyrene with organoclay: part 2 rheological properties. Polym Eng Sci 2004;44:1061–76.
[35] Tanoue S, Utracki LA, Garcia-Rejon A, Tatibouët J, Kamal MR. Melt compounding of different grades of polystyrene with organoclay: part 3 mechanical properties. Polym Eng Sci 2005;45:827–37.
[36] Utracki LA. Equations of state for polyamide-6 and its nanocomposites: 1 fundamentals and the matrix. J Polym Sci Part B Polym Phys 2009;47:299–313.
[37] Utracki LA. Equation of state of polyamide-6 and its nanocomposites: 2 effects of clay. J Polym Sci Part B Polym Phys 2009;47:966–80.
[38] Usuki A, Kawasumi M, Kojima Y, Fukushima Y, Okada A, Kurauchi T, Kamigaito O. Synthesis of PA-6-clay hybrid. J Mater Res 1993;8:1179–84.
[39] Usuki A, Kawasumi M, Kojima Y, Okada Y, Kurauchi T, Kamigaito O. Swelling behavior of montmorillonite cation exchanged for ω-amino acids by ε-caprolactam. J Mater Res 1993;8:1174–8.
[40] Stineman RW. A consistently well-behaved method of interpolation. Creat Comput 1980;6:54–7.
[41] Simha R, Boyer RF. On a general relation involving the glass temperature and coefficients of expansions of polymers. J Chem Phys 1962;375:1003–7.
[42] Simha R, Wilson PS. Thermal expansion of amorphous polymers at atmospheric pressure II theoretical considerations. Macromolecules 1973;66:908–14.
[43] Donth E. General derivation of the WLF equation from a fluctuation approach to the glass transition. Acta Polymerica 1979;308:481–5.
[44] Donth E. The size of cooperatively rearranging regions at the glass transition. J Non-Cryst Solids 1982;53:325–30.
[45] Carroll PJ, Patterson GD, Cullerton SA. Light-scattering photography of polymers near the glass transition. J Polym Sci Polym Phys Ed 1983;21(10):1889–96.
[46] Kisliuk A, Mathers RT, Sokolov AP. Crossover in dynamics of polymer liquids. J Polym Sci B Polym Phys 2000;38:2785–90.
[47] Casalini R, Roland CM. Scaling of the supercooled dynamics and its relation to the pressure dependence of the dynamic crossover and the fragility of glass formers. Phys Rev B 2005:71. 014210 (10 pg).
[48] Ngai KL. Dynamic and thermodynamic properties of glass-forming substances. J Non-Crystalline Solids 2000;275:7–51.
[49] Ngai KL. An extended coupling model description of the evolution of dynamics with time in supercooled liquids and ionic conductors. J Phys Condens Matter 2003;15:S1107–25.
[50] Stauffer D, Aharony A. Introduction to percolation theory. London: Taylor & Francis; 1992.
[51] Ballesteros HG, Fernández LA, Martin-Mayor V, Muñoz Sadupe A, Parisi G, Ruiz-Lorenzo JJ. Scaling corrections: site percolation and Ising model in three dimensions. J Phys A Math Gen 1999;32:1–13.
[52] Lorenz CD, May R, Ziff RM. Similarity of percolation thresholds on the HCP and FCC lattices. J Stat Phys 2000;98:961–70.
[53] Neher RA, Mecke K, Wagner H. Topological estimation of percolation threshold. J Stat Mech 2008:P01011.
[54] Lyngaae – Jorgensen J, Lunde Rasmussen K, Chtcherbakova EA, Utracki LA. Flow induced formation of dual – phase continuity in polymer blends and alloys. Part Polym Eng Sci. 1999;39:1060–71.
[55] Lyngaae-Jørgensen J, Utracki LA. Structuring polymer blends with bi-continuous phase morphology part II tailoring blends with ultra-low critical volume fraction. Polymer 2003;44:1661–9.
[56] Brucato V, Crippa G, Piccarolo S, Titomanlio G. Crystallization of polymer melts under fast cooling I: nucleated polyamide-6. Polym Eng Sci 1991;31:1411–6.
[57] Kojima Y, Usuki A, Kawasumi M, Okada A, Fukushima Y, Karauchi T, Kamigaito O. Mechanical properties of nylon-6 clay hybrid. J Mater Res 1993;8:1185–9.
[58] Fornes TD, Paul DR. Crystallization behavior of nylon 6 nanocomposites. Polymer 2003;44:3945–61.
[59] La Carrubba V, Brucato V, Piccarolo S. The use of master curves to describe the simultaneous effect of cooling rate and pressure on polymer crystallization. Polym Int 2004;53:61–8.
[60] Utracki LA. Compressibility and thermal expansion coefficients of nanocomposites with amorphous and crystalline polymer matrix. Eur Polym J 2009;45:1891–903.
[61] Wood LA. Glass transition temperatures of copolymers. J Polym Sci 1958;28:319–30.